A General Equivalent Electrical Circuit Model for the Characterization of MXene/Graphene Oxide Hybrid-Fiber Supercapacitors by Electrochemical Impedance Spectroscopy -Impact of fiber length

Julia Mainka, Wei Gao, Nanfei He, Jérôme Dillet, Olivier Lottin

A General Equivalent Electrical Circuit Model for the Characterization of MXene/Graphene Oxide Hybrid-Fiber Supercapacitors by Electrochemical Impedance Spectroscopy – Impact of fiber length

Julia Mainka[1*], Wei Gao[2], Nanfei He[2], Jérôme Dillet[1], Olivier Lottin[1]

1 Université de Lorraine, CNRS, LEMTA, F-54000 Nancy, France

2 Wilson College of Textiles, North Carolina State University (NCSU), 1020 Main Campus Dr Raleigh, NC 27606, United-States

* Corresponding author: julia.mainka@univ-lorraine.fr, LEMTA, 2 avenue de la Forêt de Haye, 54505 Vandœuvre-lès-Nancy, France

Keywords: Electrochemical Impedance Spectroscopy (EIS), Equivalent Electrical Circuit (EEC), Transmission Line Model (TLM), Fiber-shaped Supercapacitors (FSCs), MXene

Abstract

Performance engineering of electrochemical energy-storage devices such as Supercapacitors (SCs) requires updated modeling capable of characterizing their electrical output in unique device geometries. In this work, an Equivalent Electrical Circuit (EEC) is developed to fit the impedance data of pseudo-capacitive and electrostatic fiber-shaped supercapacitors (FSCs). The model is applied for the interpretation of impedance data measured on FSCs made of reduced Graphene Oxide (rGO) and MXene in the case of pseudo-capacitors and pure carbon in the case of Electrical Double-Layer Capacitors (EDLCs) as active electrode materials, and polyvinylalcohol (PVA) gel infiltrated with sulfuric acid as the electrolyte and separator. The FSC charge storage behavior is modeled using a Transmission Line Model (TLM) including a finite Warburg impedance for pseudo-capacitance, and a Constant-Phase Element (CPE) for the electrostatic contribution. The high frequency part of the Nyquist plots is characterized by a 45° straight line and the use of a TLM clearly improves the fit quality compared to a Randles circuit usually used for pseudo-capacitor modeling. The difference between the two circuits becomes more visible as the length of the SC yarns increases, which is consistent with the observed increase in internal resistance with fiber length evidenced with the TLM. Furthermore, the fitting results indicate that the internal resistance of the TLM predominantly corresponds to the electrical resistance of the fiber, i.e. the electron conductive phase of the electrode, instead of the electrolyte ionic resistance in usual SCs. Finally, the low frequency part of the spectra is correctly modeled by a CPE without any leakage resistance, showing that self-discharge is not a significant issue for the electrostatic contribution, at least in the frequency range tested.

1. Introduction

Supercapacitors (SCs) turned out to be efficient devices for electric energy storage thanks to their much higher energy density *vs*. classical electrostatic capacitors, and power density *vs*. batteries. In Electrical Double-Layer Capacitors (EDLCs), charges are stored in the porous electrodes in a purely capacitive manner within an Electrical Double-Layer (EDL) [1, 2]. In several cases, additional pseudo-capacitive energy storage is possible, through underpotential deposition, redox reactions and/or ion intercalation [3, 4, 5]. This is the case in SCs including 2D materials such as graphene oxide (GO) and transition metal carbides, nitrides and carbonitrides called MXenes [3, 6, 7, 8]. The energy density is thus improved but this may also

lead to durability issues due to their chemical fragility which is further increased when using unique device geometries, such as Fiber-Shaped Supercapacitors (FSCs).

The optimization of supercapacitors requires updated modeling that captures the physics at the material scale in order to characterize their electrical output. In the case of Electrochemical Impedance Spectroscopy (EIS), one way of modeling is using Equivalent Electrical Circuits (EECs), which are commonly based on the Randles circuit [9, 10, 11, 12, 13, 14, 15]. The Randles circuit is depicted in its original form in Figure 1a). It is composed of a parallel connection of a charge-transfer resistance R_{ct} and a capacitance C_{ct} representing faradaic processes. Ion diffusion is taken into account through a finite Warburg impedance Z_W connected in series to R_{ct}. The Warburg impedance writes as [10, 11]

$$\mathrm{Z_W}(\omega) = \frac{\mathrm{R_W}}{\sqrt{\mathrm{i}\omega\tau}}\tanh\sqrt{\mathrm{i}\omega\tau} \tag{1}$$

where $\mathrm{R_W}$ stands for the diffusion resistance, τ is the associated characteristic time, ω the angular frequency (in rad) and i the imaginary unit. The Warburg impdedance is associated with binary diffusion through a porous passive medium of finite length and derives from the solution of the Fick equations in the frequency domain. Eq. (1) is the most general form of the Warburg diffusion impedance, although the simplified expression corresponding to its high frequency limit $\lim_{\omega\to\infty} Z_W = \mathrm{R_W}/\sqrt{\mathrm{i}\omega\tau}$ can be encountered in the literature [4, 15]. It is worth mentionning that the derivation of the Warburg impedance is made under the assumption that diffusion is intrinsically coupled to charge-transfer in a faradaic reaction [16]. That is the reason why it is used for modeling reactant transport in electrochemical converters such as Polymer Electrolyte Membrane Fuel Cells (PEMFCs) [10, 11]. Finally, a series or high frequency resistance R_s is added to account for the various electric and connective losses. The impedance of the Randles circuit in Figure 1**Erreur ! Source du renvoi introuvable.**a) writes then [11, 14]

$$\mathrm{Z_{Randles}}(\omega) = \mathrm{R_s} + \left(\frac{1}{\mathrm{R_{ct}} + \mathrm{Z_w}(\omega)} + \mathrm{i}\omega\, C_{ct}\right)^{-1} \tag{2}$$

In the case of blocked electrodes such as for SCs, another capacitive element (C_{dl}) is also added in series as shown in Figure 1a) [15].

Figure 1b) shows the typical shape of an impedance spectrum obtained using the Randles EEC with a double-layer capacitance C_{dl} connected in series (Figure 1a)). The vertical low frequency (LF) line is obtained in the absence of a leakage resistance in parallel with C_{dl}. It is observed only with system without self-discharge. Note that in addition to self discharge, the deviation from a vertical line at low frequencies can also originate from ion diffusion, adsorption or other charge transfer processes within the porous electrodes wich results in a multitude of characteristic time constants [17, 18, 19, 20, 21]. The semi-circle at high frequencies is typical of such EEC. One common modification consists in using a constant phase elements (CPEs) Z_{CPE} instead of capacitances. Using $Z_{CPE_{ct}}$ instead of C_{ct} results in a depressed semi-circle with its center falling below the horizontal axis [12, 13]. Nonetheless, independently of the capacitive element, the shape of impedance spectra modelled with the Randles circuit is characterized by a loop in the Nyquist plot at intermediate frequencies.

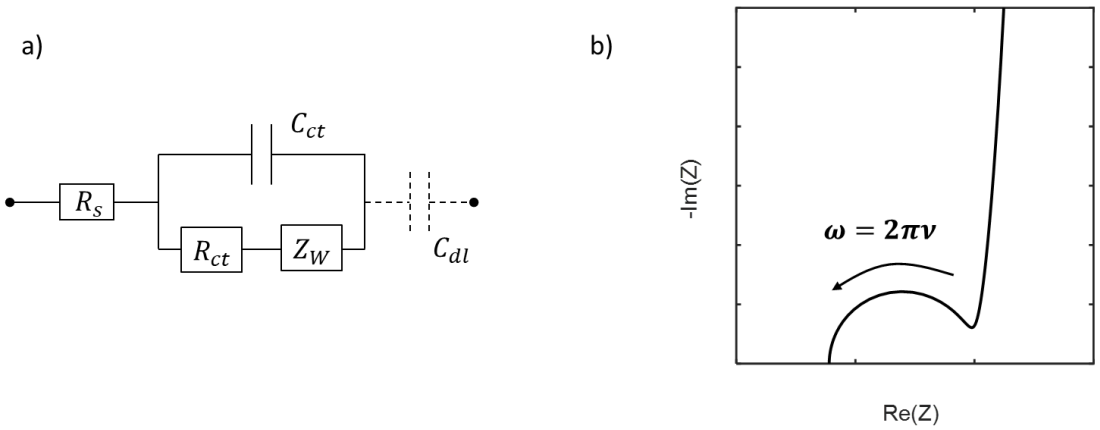

Figure 1: a) Randles equivalent electrical circuit (plain lines). The connexion in series with a double layer capacitance C_{dl} is used with blocked electrodes. b) Example of the shape of a typical spectrum in the Nyquist plot corresponding to the complete EEC in a).

However, some SC impedance spectra exhibit a 45° straight line at high frequencies in the Nyquist plot that cannot be correctly modelled using a Randles EEC. Indeed, the Randles circuit is based on the assumption of an electrochemical reaction occurring at the interface between resistive and diffusive media [12, 13]. Note that the finite Warburg impedance considered alone also has a phase angle of 45° at high frequencies [4]. However, this does not impact the overall spectra of Randles EEC: the 45° straight line observed in SC impedance spectra arises at frequencies far beyond those of the Warburg impedance.

Contrary to the Randles circuit, Transmission Line Models (TLMs) are well adapted to thick electrodes and relate the 45° straight line at high frequencies to charge transport – in general ion conduction - through their volume [4, 10, 18, 20, 22, 23, 24, 25, 26, 27] [28, 29, 30, 31]. TLMs were first introduced by de Levie for modeling the impedance of porous electrodes of EDLCs [27]. Such TLMs are composed of a network of individual RC elements accounting for capacitive charge storage in the EDL at the solid active material/liquid electrolyte interface, that are separated by internal resistances relative to charge transport (usually ion conduction) through the electrode volume [4, 20, 22, 23, 24]. The presence of faradaic processes in pseudo-capacitive SCs requires an unblocked TLM to account for a leakage or charge-transfer resistance in parallel to the capacitance [14, 18, 25, 26, 31, 32]. In addition, ion diffusion in the faradaic reaction can be modelled using a Warburg impedance connected in series to the charge-transfer resistance [9, 10, 19, 21, 33]. It can be shown that TLMs are actually a generalized form of Randles circuits for thick electrodes [10]. Finally, some impedance spectra sometimes have a HF line with a slope different from 45°: this is usually explained by inhomogeneous ion transport that may occur through thick electrodes and/or at high current densities [34].

In this work, the ability of a TLM EEC developed to fit the impedance spectra of three types of fiber-shaped SCs fabricated at the NCSU (pseudo-capacitive and EDLCs) is discussed in comparison to that of a Randles circuit. Differences lie in both the active materials and the electrical architecture of the FSCs:

- FSC1: rGO/MXene hybrid fibers twisted together as the active electrode and stainless steel filaments as current collectors.

- FSC2: two commercial 1k-carbon fiber yarns twisted together as the active electrode, with no additional current collectors.
- FSC3: activated carbon infiltrated in a single strand of 1k-carbon fiber yarn as the active electrode with no additional current collectors.

The change in the active materials is expected to have an impact mainly on the expression of pseudo-capacitive (faradaic) and electrostatic contributions in the impedance of the devices. Therefore, the impedance model is designed to account for both contributions. It is shown that only the impedance spectra of short SC yarns ($< 5\ cm$ for the herein called FSC1 devices) can be fitted using a Randles circuit, this because the potential drop along the fibers becomes significant when their length increases. A TLM seems thus more adapted than a Randles circuit as it takes the charge transport along the fiber length into account, through the internal resistance [4, 20, 22, 23, 24]. This expectation is confirmed as the internal resistance of FSC1 devices increases with the fiber length. Furthermore, it turns out that the internal resistance of the TLM corresponds mainly to the electronic resistance of the fibers rather than to the ionic resistance of the electrolyte, which is the opposite of what is observed with more common devices [4, 10, 18, 20, 22, 23, 24, 25, 26, 27] [28, 29, 30, 31]. Finally, the low frequency part of the spectra was correctly fitted using a CPE without the need to connect a leakage resistance in parallel indicating that self-discharge is not an issue for electrostatic charge storage, at least in the tested frequency range.

2. Experimental

The experimental data underlying this work are obtained using fiber-shaped SCs with different electrode materials fabricated by wet-spinning, as explained in [9].

2.1. Fiber-shaped SuperCapacitors 1 - FSC1

The devices denoted FSC1 in the following have electrodes made of a mixture of rGO and MXene. MXenes are two-dimensional early transition metal carbides, nitrites and carbonitrides obtained by selective etching of layered ternary transition metal carbides -MAX phases- in acidic fluoride containing solutions [35]. The resulting MXenes have a general formula $M_{n+1}X_nT_x$, with M the transition metal, X the C and/or N atoms, n an integer varying between 3 and 1, and T_x representing the surface functional groups. The MXene used here is titanium carbide Ti_3C_2X, X corresponding to -O, -OH or –F. Due to their particular 2D-shaped structure and composition, three types of charge storage mechanisms (faradaic, EDL and ion-intercalation) are observed in SCs including MXene, the extent of each contribution depends on the electrode components and electrolyte type [7, 36, 37].

A Scanning Electron Microscopy (SEM) image, as well as a scheme of the electrode cross-sectional structure and connection are depicted in Figure 2. Each electrode is composed of one ‘dual-core’ rGO/MXene yarn coated with gel electrolyte. The weight ratio of active material is 40wt% rGO and 60wt% MXene. The rGO/MXene fibers are soaked for a few hours in 1 M sulfuric acid (H_2SO_4)/Polyvinyl alcohol (PVA) solution to ensure satisfying diffusion of the electrolyte between the rGO and MXene flakes. Subsequently 4 rGO/MXene fibers are assembled around a stainless steel filament that acts as the current collector. This means that each electrode contains 8 rGO/MXene fibers and 2 stainless-steel filaments. The diameter of one single rGO/MXene fiber is of about $50\ \mu m$, resulting in a diameter of about $500\ \mu m$ for one electrode. The entire device is composed of 2 identical electrodes twisted together as

shown in Figure 2b). If not mentioned otherwise, data are measured on 15 cm-long yarns that serve as reference case for the EEC model derivation.

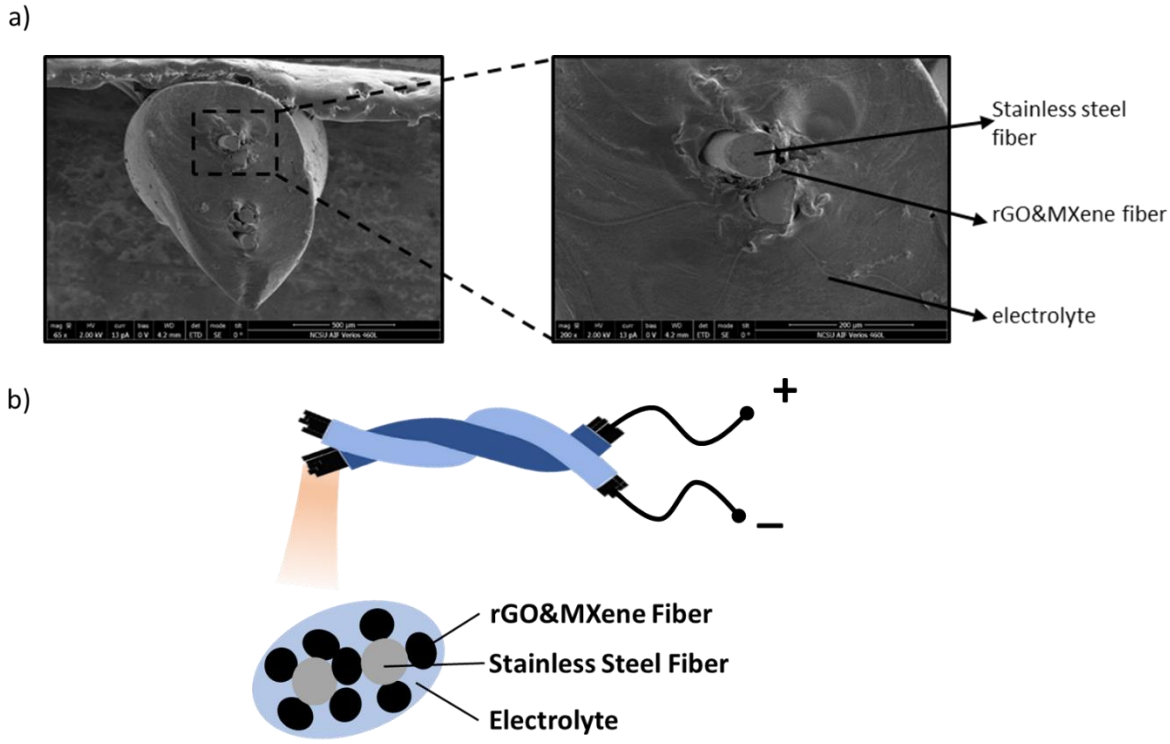

Figure 2: a) SEM image and b) scheme of the electrode cross-sectional structure and the electrical connection of a FSC1 device including. Each electrode is composed of one 'dual-core' rGO/MXene yarn coated with gel electrolyte (8 rGO/MXene fibers and 2 stainless-steel filaments in each electrode). Electric connections are on the same side in both cases.

2.2. Fiber-shaped SuperCapacitors 2 and 3 (FSC2 and FSC3)

Devices FSC2 and FSC3 have electrodes made of pure 1k carbon yarns that are commercially available. FSC2 uses two of 1k-carbon yarns in one electrode, where the two 1k-carbon yarns are twisted to form one electrode. FSC3 have electrodes made of a single strand of 1k-carbon yarn infiltrated with activated carbon, with only 1 yarn per electrode. The electrolyte is a 1 M sulfuric acid (H_2SO_4)/Polyvinyl alcohol (PVA) gel. The diameter of a single 1k carbon yarn is of about 110 μm, resulting in a diameter of about 155 ± 5 μm per electrode of FSC2 and 160 ± 5 μm per electrode of FSC3. The length of these devices is always 15 cm.

Current collection is done at the same end for all devices as depicted in Figure 2b).

The model derivation is based on impedance data measured in potentiostatic mode with a perturbation amplitude limited to $10mV$ (peak to peak) around $0\,V$ voltage in a frequency range between 10 mHz and 1 MHz.

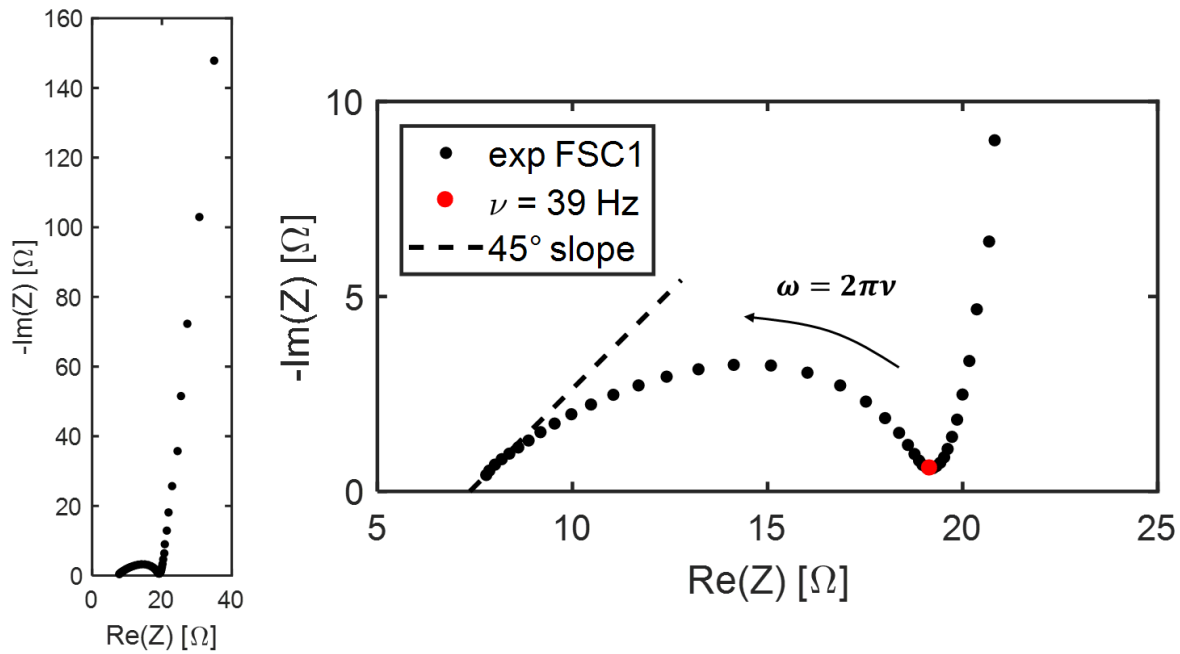

Figure 3: Nyquist plot of an impedance data of the FSC1 (15 cm) measured with a perturbation amplitude of $10mV$ (peak to peak) around 0V for frequencies ν ranging from 1mHz to 1MHz.

Figure 3 shows the Nyquist plot of a $15\ cm$ FSC1 impedance spectrum. The spectrum consists of a straight line at the highest frequencies (HFs) typically associated with ion conduction through the electrode pores [27, 28, 29, 30]. In the case of the fiber-shaped SCs, this HF straight line might be associated with the electronic resistance rather than the ionic resistance as for conventional SC: indeed, the electric transfer limitations are governed by the length of the yarns rather than, usually, the electrode thickness. This point will be addressed in the discussion section. At intermediate frequencies (IFs) the spectrum is characterized by a depressed semi-circle typical of faradaic charge transfer [4, 10, 11, 19, 21, 25]. Finally, the imaginary part of the SC impedance steeply increases at low frequencies, which is a signature of electrostatic charge storage such as EDL or ion-intercalation. The frequency relative to the transition between pseudocapacitive and electrostatic regimes is close to $39\ Hz$. According to the shape of this EIS spectrum, there seems to be both electrostatic [5] and faradaic [3, 6, 21] charge storage, which is in agreement with the expectations for SCs incorporating MXene in acidic electrolyte: charge storage should primarily be due to redox processes [7, 8, 36, 37], but Zhan et al. [7] showed recently that the redox process was primarily due to Ti valence change and competed with electrostatic storage.

Figure 4 shows the impedance spectra measured on a) FSC2 and b) FSC3. With pure carbon electrodes, an EDLC-like behavior is expected, *i.e*. without IF loop, a 45° inclined line at HFs, and a vertical line at LFs. Their impedance spectra serve thus for comparison with FSC1 with an additional pseudo-capacitive behavior due to their rGO/MXene electrodes. As for FSC1, the imaginary part of the impedance spectra steeply increases at LFs linked to electrostatic charge storage, most probably in the EDL. The depressed semi-circle at IFs is however absent in these spectra, which is in agreement with the expectations for EDLCs [27, 38]. Finally, the inclined line at HFs is associated with charge conduction through the electrodes. The transition between the HF and LF regimes occurs at frequencies around $120\ Hz$ for FSC2 and $240\ Hz$ for FSC3. Interestingly, the FSC3 impedance spectra (Figure 4 b)) exhibit two inclined segments in

the LF region with a slope change at $0.6\ Hz$ which is typical for activated carbon sample and might be linked with the wide range of pore-size distribution.

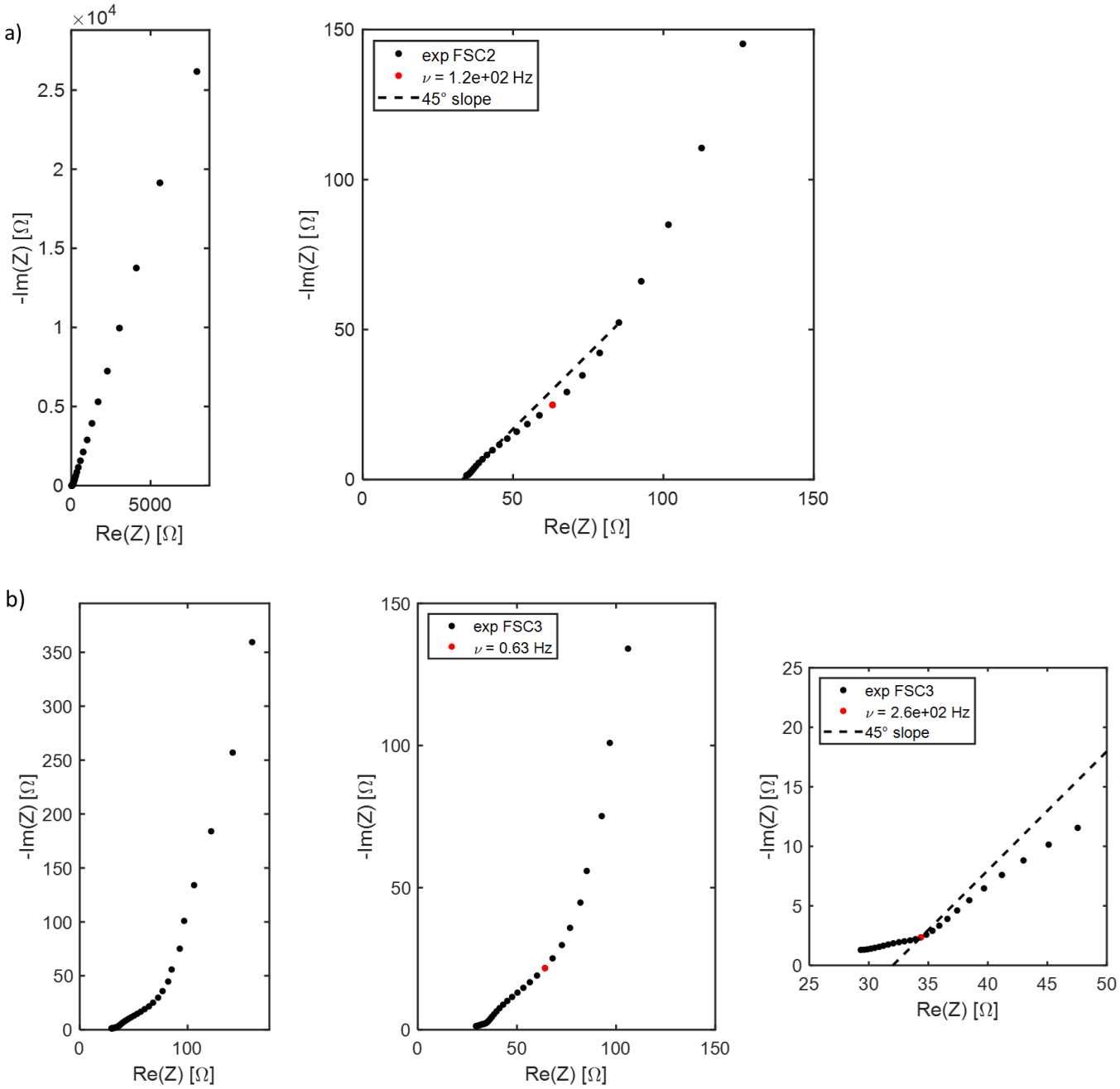

Figure 4: Nyquist plot of impedance data of a) FSC2 and b) FSC3, both 15 cm in length, measured with a perturbation amplitude of $10mV$ (peak to peak) around 0V for frequencies ν ranging from 1mHz to 1MHz.

3. Theory

The EECs used in this work were developed to fit the impedance spectra of the fiber-shaped SCs fabricated at the NCSU. The requirements of the model were twofold: being sufficiently detailed to capture the main physics at the material scale while remaining sufficiently simple to be used for *in-situ* characterization.

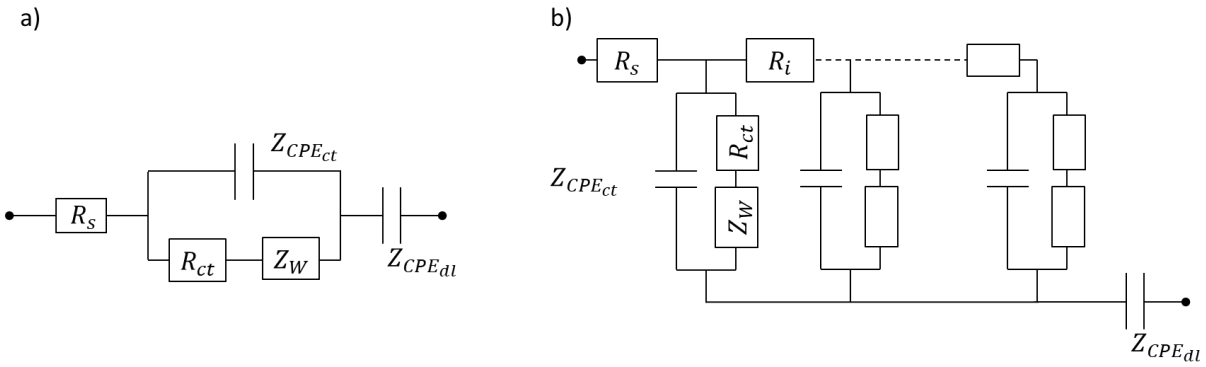

Figure 5: Equivalent Electrical Circuits used for fitting the impedance spectra of the FSCs consisting of a series resistance R_s, and a) a Randles-like or b) a TLM EEC representing faradic charge storage in thin or volumetric electrodes, respectively. A double-layer CPE_{dl} is connected in series to account for electrostatic charge storage.

As discussed in the introduction (Figure 1) Randles-like EECs are unable to reproduce the 45° straight line observed in the high-frequency domain of the impedance spectra of the fiber SCs. This is why a Transmission Line Model was adopted [10, 14, 27, 32]. Recent improvements on TLMs made it possible to include diffusion limitations under the form of a Warburg impedance [10, 31]. The resulting circuit is shown in Figure 5b): it consists of an infinite network of Randles circuits connected to each other via internal resistances R_i accounting for charge conduction within the electrode. As mentioned earlier, in conventional SCs the electronic resistance of the active material is negligible compared to the ionic resistance of the electrolyte and R_i is associated with ion conduction [4, 10, 18, 20, 22, 23, 24, 25, 26, 27] [28, 29, 30, 31]. In the present case however, the main direction of electronic conduction being the yarn length, it is expected that the electronic resistance dominates the ionic resistance (through the yarn thickness).

Under the assumption of homogeneous electric properties, the TLM impedance writes [10]

$$Z_{TLM}(\omega) = \sqrt{\frac{R_i \times (R_{ct} + Z_W(\omega))}{1 + \frac{R_{ct} + Z_W(\omega)}{Z_{CPE_{ct}}(\omega)}}} \coth\left(\sqrt{\frac{R_i}{R_{ct} + Z_W(\omega)}\left(\frac{R_{ct} + Z_W(\omega)}{Z_{CPE_{ct}}(\omega)} + 1\right)}\right) \qquad (3)$$

It can be shown that this TLM is a generalization of the Randles circuit for volumic electrodes [10]: i.e. thick, instead of thin flat electrodes in the case of usual SC or long, rather than short yarns in the present case. When R_i becomes zero, the TLM impedance of Eq.(3) tends to that of the Randles circuit Eq.(2). Here, a constant phase element $Z_{CPE_{ct}}$ is used instead of a pure capacitance.

Eq.(3) applies to electrodes with pure pseudo-capacitive charge storage. However, the experimental spectra (Figure 3 and Figure **4**) exhibit an inclined straight line at low frequencies indicating an additional electrostatic contribution. Eq.(3) was therefore completed by adding a double-layer constant phase element $Z_{CPE_{dl}}$ in series to the faradaic circuit. It accounts for electrostatic charge storage as a whole -*via* the EDL and/or possibly ion intercalation for electrodes including MXene-, the extent of each contribution being still unclear [7]. This additional capacitive element is required to correctly fit the experimental data.

It is usual in the literature to connect a resistance in parallel to $Z_{CPE_{dl}}$ to account for self-discharge [15, 22, 39]. In our case however, adding a resistance did not improve the fit of the experimental data for any of the tested devices, suggesting that self-discharge is not a significant issue, at least not in the frequency range that was tested. Therefore, only a CPE was used for the electrostatic component to keep the number of parameters as low as possible.

Finally, a series or high frequency resistance R_s was added. It accounts for the various electric and connective losses, including the resistance related to the electrostatic charge storage linked with $Z_{CPE_{dl}}$ (Figure 5). The resulting overall impedance is thus

$$\mathrm{Z}_{SC}(\omega) = \mathrm{R_s} + \mathrm{Z}_{TLM/Randles}(\omega) + Z_{CPE_{dl}}(\omega) \tag{4}$$

with the CPE impedance being given by [4, 40]

$$Z_{CPE_{ct/dl}} = \frac{1}{(\mathrm{i}\omega)^{\alpha_{ct/dl}}\mathrm{Q}_{ct/dl}} \tag{5}$$

and $0 \leq \alpha_{ct/dl} \leq 1$ is the CPE exponent and $Q_{ct/dl}$ the CPE magnitude or apparent capacitance (in $F.s^{-\alpha}$). CPEs allow to enhance the fit quality of Nyquist plots showing a depressed semi-circle centered below the x-axis that cannot be properly simulated with classical capacitances. This is often the case with porous electrodes, like in fuel cells and pseudo-capacitive SCs [4, 9, 19, 21, 41]. Nevertheless, discussion remains about the physical meaning of CPEs, with explanations being often linked to the porous nature of the electrodes such as surface roughness [42, 43], fractal dimension [44, 45] or pore size distribution [46]. Niya et al. [40] used anomalous diffusion theory to derive analytically the expression of the CPE impedance. They demonstrated that the CPE exponent α is equal to the subdiffusion power and can give information about the impact of the porosity on ion diffusion. The case $\alpha = 1$ corresponds to normal diffusion and the CPE impedance then takes the form of a pure capacitance. The lower the value of α the more pronounced the impact of the pore space on diffusion. We observed that CPEs are required in the present case to obtain a satisfying fit and interpretation will be done in comparison to normal diffusion ($\alpha = 1$). Note that although not being relevant for supercapacitor applications, inductive elements ($\alpha = -1$) associated with the electric connection are sometimes added to the impedance model (e.g. [38]) in order to improve the estimation of the high frequency resistance R_s. However, they did not impact the fit quality nor the parameter estimation in the present case and were thus omitted to keep the model as simple as possible.

4. Results and Discussion

In this section, the ability of the two EECs of Figure 5 to fit the impedance data of the FSCs presented above is discussed.

4.1. FSC1 data set

Figure 6 shows the data measured for the FSC1 devices and the corresponding fitting curves. The blue line is obtained with the Randles-type EEC (Figure 5a)), while the red one corresponds to the TLM circuit (Figure 5b)). The estimated model parameters are given in Table 1.

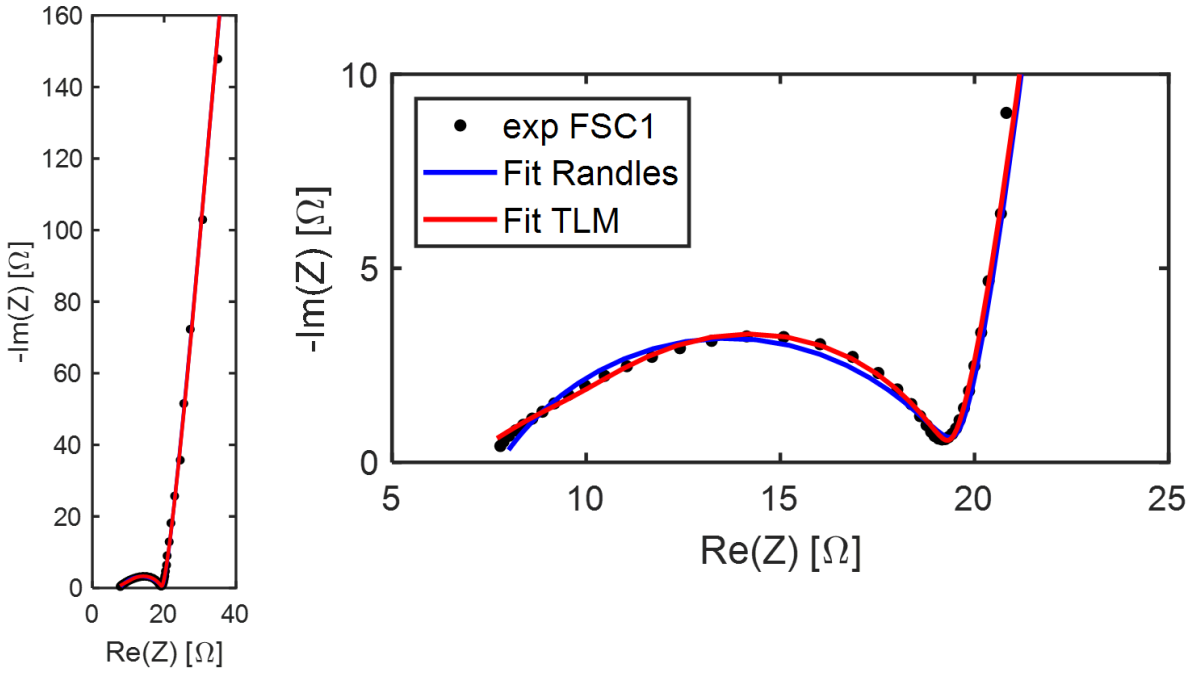

Figure 6: Nyquist plot of the impedance data measured for FSC1 devices shown in Figure 3 and fitting curves obtained with the Randles (blue) and the TLM (red) EECs, respectively. Left: overall spectrum; right: close-up to high frequencies.

	R_s	R_i	R_{ct}	Q_{ct}	α_{ct}	R_W	τ	Q_{dl}	α_{dl}
	[Ω]	[Ω]	[Ω]	[$\mu F.s^{-\alpha ct}$]	[-]	[Ω]	[s]	[$mF.s^{-\alpha dl}$]	[-]
Randles	7.8	-	11.7	120	0.64	20.2	64.1	47.5	0.96
TLM	6.8	9.4	9.6	67	0.74	22.8	62.9	48.0	0.96
Difference [%]	15	-	22	79	-14	-11	2	-1	-0.2

Table 1: Impedance parameters estimated on the impedance spectrum of the pseudo-capacitive yarns, *i.e.* FSC1 shown in Figure 6.

The discussion is done by considering separately the intermediate to high frequency part (*i.e*. the loop) and the low frequency part (*i.e*. the inclined line) of the spectrum.

There is no remarkable difference in the fitting curves at low frequencies (left side of Figure 6). Indeed, electrostatic charge storage associated with the LF region is modeled identically in both EECs by a constant phase element $Z_{CPE_{dl}}$. Consistently, both EECs yield comparable parameters of about $48 \pm 0.5\ mF.s^{-\alpha_{dl}}$ for Q_{dl} and 0.96 for α_{dl}. The CPE exponent is close to 1, indicating an almost ideal capacitive behavior. As mentioned above, the LF part is correctly modeled by $Z_{CPE_{dl}}$ without any leakage resistance.

On the contrary, the fit of the loop depends on the type of pseudo-capacitive EEC (TLM or Randles) as can be seen on the right side of Figure 6. Despite using a CPE, the Randles cicuit is unable to correctly fit the 45° straight line at the highest frequencies. The TLM allows a better fit of both the HF inclined line as well as the depressed semi-circle at IFs. This difference in the fitting curves is also observed for the impedance parameters associated with the pseudo-

capacitive EEC, i.e. R_{ct} and Q_{ct}, α_{ct}, R_W and τ, for which we observe differences of 22%, 79%, 14%, 11% and 2% respectively in comparison with the TLM parameters. The characteristic time of the Warburg impedance τ is the parameter that is the less affected. The CPE exponent α_{ct} is estimated by the TLM EEC to be 0.74 indicating a more important impact of the porositiy on pseudo-capacitive than on electrostatic charge storage. Finally, as the TLM gives a better fit at high frequencies, it allows a better estimation of the series resistance R_s. The importance of using a TLM instead of Randles EEC becomes more obvious when the HF 45° straight line is more developped, which is the case for longer fibers SCs, as shown in Figure 7a). The HF 45° line is linked to the internal resistance R_i which increases with the fiber length, as shown on Figure 7b) (left side).

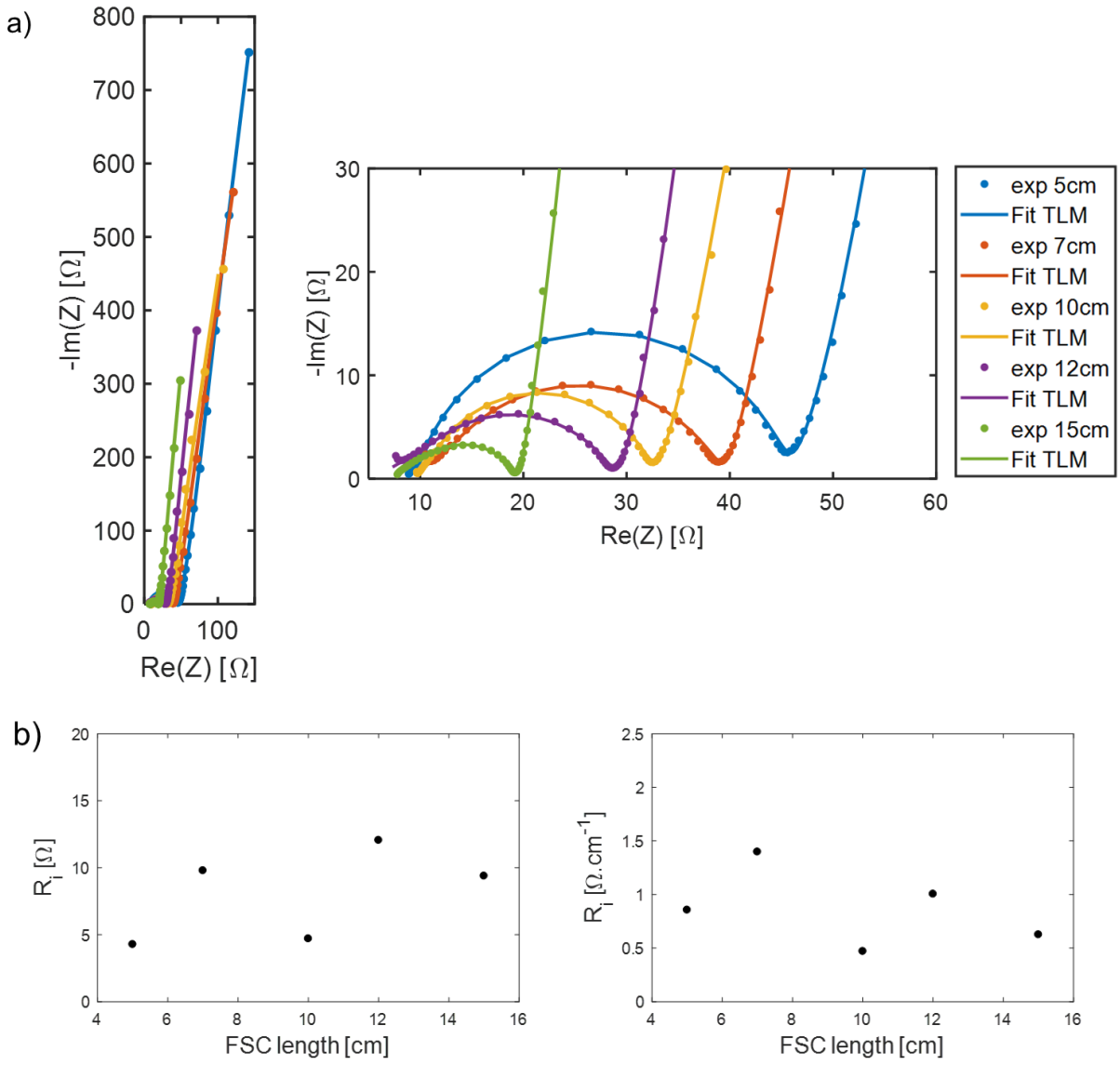

Figure 7: a) Nyquist plot of the impedance spectra measured on FSC1 of different length. The fitting curves were obtained using the TLM EEC of Figure 5b). Left: overall spectra; right: close-up to high frequencies. b) Internal resistance absolute value (left) and per unit length (right) identified from the fitting curves of a).

The internal resistance R_i of the TLM is $9.4\ \Omega$ for the $15\ cm$ long device, or $0.63\ \Omega.cm^{-1}$ which is of the order of the electrical resistance of the rGO/MXene mixture, i.e. $1.19\ \Omega.cm^{-1}$. The same order of magnitude is obtained by fitting the fibers of different lengths as shown in Figure 7b). This confirms that R_i is governed by the electron conducting phase of the electrode (here rGO/MXene) rather than the ion conductive electrolyte. This is different from classical SCs where the electrolyte is the most limiting material in terms of charge condution, but easily explained by the fiber-shape of the devices.

Four conclusions can be drawn from this comparison:

I. Both pseudo-capacitive and electrostatic charge storage have to be considered in the impedance model.

II. No improvement has been observed when connecting a leakage resistance in parallel to $Z_{CPE_{dl}}$: self-discharge is either not an issue for electrostatic charge storage with these FSCs or does not manifest itself in the frequency range that has been tested.

III. The faradaic contribution is significantly affected by charge transport inside the electrode, as can be seen through the 45° straight line at the highest frequencies; the longer the fibres, the more pronounced this effect. . Therefore, a TLM (Figure 5b)) has to be used to correctly fit the impedance spectra of all devices. Using a Randles EEC (Figure 5a)) gives satisfying results only for short fibers ($\leq 5\ cm$).

4.2. FSC2 and FSC3 data set

In order to test the validity of the EECs for a characterization of EDLCs, they have been used to fit the data of FSC2 and FSC3. The corresponding curves are shown in Figure 8. The model parameters estimated with the TLM EEC are summarized in Table 2 .

As for FSC1, there is no remarkable difference in the fitting curves between the Randles and TLM circuits at low frequencies (left side of Figure 8 a) and b)), which is consistent with the use of a constant phase element $Z_{CPE_{dl}}$ in both EECs to account for electrostatic charge storage. Again, the LF data are correctly modeled by $Z_{CPE_{dl}}$ without any leakage resistance and the CPE exponent α_{dl} is close to 1, indicating an almost ideal capacitive behavior.

The TLM fitted satisfactorily the impedance data of FCS2 and FCS3 in both the IF and HF domains, whereas the Randles-like EEC was unable to fit the impedance at these frequencies. This is more pronounced for the spectra of FSC2 (Figure 8a)) than for those of FSC3 (Figure 8b)), and consistent with the presence of a weakly developed depressed semi-circle (FSC3) or its absence (FSC2), since it is associated with faradaic reactions. On a modeling point of view, this is linked with relatively high values of the electrode resistances R_{ct} and R_W, which were estimated to $33.0\ \Omega$ and $56.3\ \Omega$ for FSC2 and $23.6\ \Omega$ and $219.6\ \Omega$ for FSC3. The associated CPE exponent α_{ct} is close to 1 for FSC2, whereas it is about 0.01 for FSC3 indicating a more significant impact on the porosity on charge transport through the electrodes when using activated carbon in addition to 1k carbon.

Finally, the series resistance R_s estimated by the TLM with the FSC3 data (Figure 8b)) was close to zero, indicating low or negligible contact resistances.

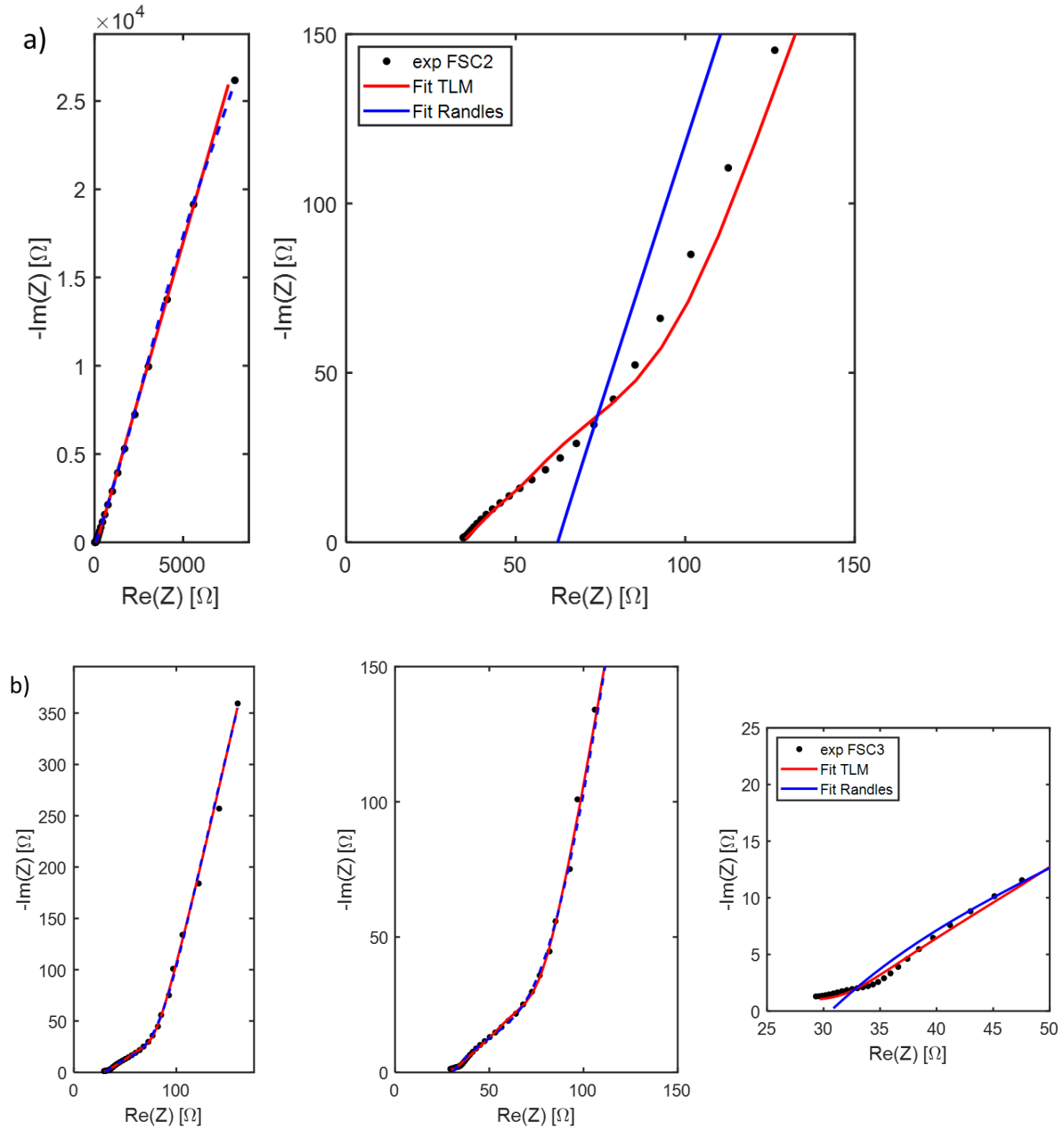

Figure 8: Nyquist plot of the impedance data measured on a) FSC2 and b) FSC3 shown in Figure 4 and fitting curves obtained with the Randles (blue) and TLM (red) EEC, respectively. Left: overall spectrum; center and right: close-up to intermediate and high frequencies.

	R_s	R_i	R_{ct}	Q_{ct}	α_{ct}	R_W	τ	Q_{dl}	α_{dl}
	[Ω]	[Ω]	[Ω]	[$\mu F.s^{-\alpha ct}$]	[-]	[Ω]	[s]	[$mF.s^{-\alpha dl}$]	[-]
FSC2	34.1	56.3	33.0	0.1	0.96	56.3	0.18	0.4	0.82
FSC3	$1.3\ 10^{-6}$	67.6	23.6	14.5	0.08	219.6	1.1	30.7	0.86

Table 2: Impedance parameters estimated with the TLM circuit on the impedance spectra of the EDLC yarns, *i.e.* FSC2 and FSC3 shown in Figure 8.

The internal resistance R_i of the TLM EEC is of the order of $56.3\ \Omega$ or $3.7\ \Omega.cm^{-1}$ for FSC2, and $67.6\ \Omega$ or $4.5\ \Omega.cm^{-1}$ for FSC3. This is close to carbon electrical resistances, *i.e.* $2.5\ \Omega.cm^{-1}$ for FSC2 and $4.7\ \Omega.cm^{-1}$ for FSC3 and confirms again that R_i is governed by the electron conductive material of the electrodes (here carbon) .

In summary, the analysis of the impedance data of the carbon SC yarns (FSC2 and FSC3, EDLCs) confirm the observations made with the rGO/MXene devices (FSC1, pseudo-capacitors), *i.e.* that both pseudo-capacitive and electrostatic charge storage have to be included in the impedance model to correctly fit the experimental data.

5. Conclusion

An Equivalent Electrical Circuit (EEC) of general use was developped to fit the impedance spectra of Fiber-shaped SuperCapacitors (FSCs). This model can be applied to Electrical Double-Layer Capacitor (EDLC) as well as pseudo-capacitive SC yarns made at the NCSU. FSCs with electrodes made of mixtures of reduced Graphene Oxide (rGO) and MXene in the case of pseudo-capacitors as well as pure carbon electrodes in the case of EDLCs were tested. The Nyquist plots were composed of a depressed semi-circle at intermediate frequencies and an inclined straight line at low frequencies, the extent of each contribution depending on the active electrode material: the faradaic loop almost vanished in the case of the carbon yarns. At the highest frequencies the spectra exhibited a 45° straight line, which is typical of thick electrodes in planar or cylindrical supercapacitors, but was herein linked to the length of the yarns.

The proposed impedance model is composed of a Transmission Line Model (TLM) including a Warburg impedance for the pseudo-capacitive contribution connected in series to a Constant-Phase Element (CPE) for electroctatic charge storage. Finally, a series resistance is needed to account for the various electric and connection resistances.

The main conclusions are:

I. Both the TLM and the CPE have to be included in the impedance model to correctly fit the data, independently of the nature of the FSCs.

II. In the presence of the 45° line at high frequencies, the use of a TLM clearly improves the fit quality compared to a Randles circuit as it accounts for charge transport along the fiber length though an internal resitance R_i. As expected, the difference between the two models becomes more visible as the length of the SC yarns and thus the internal resistance increases.

III. It was confirmed that the internal resistance R_i in the TLM corresponds to the electrical resistance of the electron conductive phase of the electrode, *i.e*. carbon in the case of EDLCs and rGO/MXene for the pseudo-capacitor yarns.

IV. The low frequency part of the spectra is correctly modeled by a CPE without connecting a leakage resistance in parallel, showing that self-discharge (or possibly ion diffusion, adsorption or other charge transfer processes within the porous electrodes) is not a significant issue for electrostatic charge storage, at least in the tested frequency range.

The next steps in the model optimization will concern the discrimination between the respective roles of EDL and ion intercalation in the electrostatic part and the identification of

the apparent real capacitance. It would also be interesting to test the application of the TLM EEC in the time domain, *i.e.* on the charging/discharging curves. On a more practical level, the model will be applied to characterize the fiber SCs as a function of the electrode formulation, their length as well as the number of yarns per electrode and electrical connexion.

Funding: This work was funded by the European Fund for Economic and Regional Development FEDER.

References

[1] L. Zubieta and R. Bonert, "Characterization of double-layer capacitors for power electronics applications," *IEEE Transactions on Industry Applications,* vol. 36, pp. 199-205, 2000.

[2] R. German, A. Hammar, R. Lallemand, A. Sari and P. Venet, "Novel experimental identification method for Supercapacitor Multi-Pore Model in order to monitor the State of Health," *IEEE Transaction on Power Electronics,* vol. 31, no. 1, pp. 548-559, 2016.

[3] M. Boota, B. Anasori, C. Voigt, M. Q. Zhao, M. W. Barsoum and Y. Gogotsi, "Pseudocapacitive Electrodes Produced by Oxidant-Free Polymerization of Pyrrole between the Layers of 2D Titanium Carbide (MXene)," *Adv. Mater.,* vol. 28, pp. 1517-1522, 2016.

[4] L. M. Da Silva, R. Cesar, C. M. Moreira, J. H. Santos, L. G. De Souza, B. Morandi Pires, R. Vicentini, W. Nunes and H. Zanin, "Reviewing the fundamentals of supercapacitors and the difficulties involving the analysis of the electrochemical findings obtained for porous electrode materials," *Energy Storage Mater.,* vol. 27, pp. 555-590, 2020.

[5] B. E. Conway, Electrochemical Supercapacitors: Scientific Fundamentals and Technological Applications, Springer US, 1999.

[6] J. Zhang, S. Seyedin, S. Qin, Z. Wang, S. Moradi, F. Yang, P. A. Lynch, W. Yang, J. Liu, X. Wang and J. M. Razal, "Highly Conductive Ti3C2Tx MXene Hybrid Fibers for flexible and elastic Fiber-Shaped Supercapacitors," *Small,* vol. 15, p. 1804732, 2019.

[7] C. Zhan, M. Naguib, M. Lukatskaya, P. R. C. Kent, Y. Gogotsi and D. Jiang, "Understanding the MXene Pseudocapacitance," *J. Phys. Chem. Lett.,* vol. 9, pp. 1223-1228, 2018.

[8] X. Mu, D. Wang, F. Du, G. Chen, C. Wang, Y. Wei, Y. Gogotsi, Y. Gao and Y. Dall'Agnese, "Revealing the Pseudo-Intercalation Charge Storage Mechanism of MXenes in Acidic Electrolyte," *Adv. Funct. Mater.,* p. 1902953, 2019.

[9] N. He, Q. Pan, Y. Liu and W. Gao, "Graphene-Fiber-Based Supercapacitors Favor N-Methyl-2-pyrrolidone/Ethyl Acetate as the Spinning Solvent/Coagulant Combination," *ACS Appl. Mater. Interfaces,* vol. 9, pp. 24568-24576, 2017.

[10] S. Touhami, J. Mainka, J. Dillet, S. Ait Hammou Taleb and O. Lottin, "Transmission Line Impedance Models Considering Oxygen Transport Limitations in Polymer Electrolyte Membrane Fuel Cells," *J. Electrochem. Soc.,* vol. 166, no. 15, pp. F1209-F1217, 2019.

[11] J. Mainka, G. Maranzana, J. Dillet, S. Didierjean and O. Lottin, "Effect of Oxygen depletion along the air channel of a PEMFC on the Warburg Diffusion Impedance," *J. Electrochem. Soc.,* vol. 157, no. 11, pp. B1561-B1568, 2010.

[12] T. Berning and N. Djilali, "3D, multiphase, multicomponent model of the cathode and anode of a PEM fuel cell," *J. Electrochem. Soc.,* vol. 150, no. 12, pp. A1589-A1598, 2003.

[13] U. Passaogullari and C.-Y. Wang, "Two-phase transport and the role of micro-porous layer in polymer electrolyte fuel cells," *J. Electrochem. Soc.,* vol. 151, no. 3, pp. A399-A406, 2004.

[14] P. M. Gomadam and J. W. Weidner, "Analysis of electrochemical impedance spectroscopy in proton exchange membrane fuel cells," *Int. J. Energ. Res.,* vol. 29, no. 12, pp. 1133-1151, 2005.

[15] C. Masarapu, H. F. Zeng, K. H. Hung and B. Wei, "Effect of Temperature on the Capacitance of Carbon Nanotube Supercapacitors," *ACS Nano,* vol. 3, no. 8, pp. 2199-2206, 2009.

[16] A. Lasia, Electrochemical Impedance Spectroscopy and its Applications, New York: Springer New York, 2014.

[17] H.-K. Song, J.-H. Sung, Y.-H. Jung, K.-H. Lee, L. H. Dao, M.-H. Kim and H.-N. Kim, "Electrochemical Porosimetry," *J. Electrochem. Soc.,* vol. 151, pp. E102-, 2004.

[18] D. I. Abouelamaiem, G. He, T. P. Neville, D. Patel, S. Ji, R. Wang, I. P. Parkin, A. B. Jorge, M.-M. Titirici, P. R. Shearing and D. J. Brett, "Correlating electrochemical impedance with hierachical structure for porous carbon-based supercapacitors using a truncated transmission line model," *Electrochim. Acta,* vol. 284, pp. 597-608, 2018.

[19] P. A. Basnayaka, M. K. Ram, L. Stefanakos and A. Kumar, "Graphene/Polypyrrole Nanoomposite as electrochemical Supercapacitor Electrode: Electrochemical Impedance Studies," *Graphene,* vol. 2, pp. 81-87, 2013.

[20] S. Fletcher, V. J. Black and I. Kirkpatrick, "A universal equivalent circuit for carbon-based spuercapacitors," *J. Solid State Electrochem.,* vol. 18, pp. 1377-1387, 2014.

[21] P. Navalpotro, M. Anderson, R. Marcilla and J. Palma, "Insights into the energy storage mechanism of hybrid supercapacitors with redox electrolytes be electrochemical Impedance Spectroscopy," *Electrochim. Acta,* vol. 263, pp. 110-117, 2018.

[22] L. Zhang, X. Hu, Z. Wang, F. Sun and D. G. Dorrell, "A review of supercapacitor modeling, estimation, and applications: A control/management perspective," *Renew. Sust. Energ. Rev.,* vol. 81, pp. 1868-1878, 2018.

[23] C. Turpin, D. Van Laethem, B. Morin, O. Rallières, X. Roboam, O. Verdu and V. Chaudron, "Modelling and analysis of an original direct hybridization of fuel cells and ultracapacitors," *Math. Comput. Simulat.,* vol. 131, pp. 76-87, 2017.

[24] F. Rafik, H. Gualous, R. Gallay, R. Crausaz and A. Berthon, "Frequency, thermal and voltage supercapacitor characterization and modeling," *J. Pow. Sourc.,* vol. 165, pp. 928-934, 2007.

[25] A. Allagui, T. J. Freeborn, A. S. Elwakil, M. E. Fouda, B. J. Maundy, A. G. Radwan, Z. Said and M. A. Abdelkareem, "Review of fractional-order electrical characterization of supercapacitors," *J. Pow. Sourc.,* vol. 400, pp. 457-467, 2018.

[26] J. Bisquert, "Influence of the boundaries in the impedance of porous film electrodes," *Phys. Chem. Chem. Phys.,* vol. 2, pp. 4185-4192, 2000.

[27] R. De Levie, "On porous electrodes in electrolyte solutions: I. Capacitance effects," *Electrochim. Acta,* vol. 8, pp. 751-780, 1963.

[28] I. D. Raistrick, "Impedance studies of porous electrodes," *Electrochim. Acta,* vol. 35, no. 10, pp. 1579-1586, 1990.

[29] J. H. Jang and S. M. Oh, "Complex Capacitance Analysis of Porous Carbon Electrodes for Electric Double-Layer Capacitors," *J. Electrochem. Soc.,* vol. 151, no. 4, pp. A571-A577, 2004.

[30] M. Eikerling and A. A. Kornyshev, "Electrochemical impedance of the cathode catalyst layer in polymer electrolyte fuel cells," *J. Electroanal. Chem.,* vol. 475, no. 2, pp. 107-123, 1999.

[31] S. Cruz-Manzo and R. Chen, "A generic electrical circuit for performance analysis of the fuel cell cathode catalyst layer through electrochemical impedance spectroscopy," *J. Electroanal. Chem.,,* vol. 694, pp. 45-55, 2013.

[32] R. De Levie, "On porous electrodes in electrolyte solutions - IV," *Electrochim. Acta,* vol. 9, no. 9, pp. 1231-1245, 1964.

[33] E. Warburg, "Ueber das Verhalten sogenannter unpolarisierbarer Elektroden gegen Wecheslstrom," *Annalen der Physik,* vol. 303, no. 3, pp. 439-499, 1899.

[34] S.-J. Lee and S. Pyun, ", Effect of annealing temperature on mixed proton transport and charge transfer-controlled oxygen reduction in gas diffusion electrode," *Electrochim. Acta,* vol. 52, pp. 6522-6533, 2007.

[35] M. Naguib, V. Mochalin, M. W. Barsoum and Y. Gogotsi, "MXenes: A New Family of Two-Dimensional Materials," *Adv. Mater.,* vol. 26, pp. 992-1004, 2014.

[36] M. R. Lukatskaya, S.-M. Bak, X. Yu, X.-Q. Yang, M. W. Barsoum and Y. Gogotsi, "Probing the Mechanism of High Capacitance in 2D Titanium Carbide Using In Situ X-Ray Absorption Spectroscopy," *Adv. Energy Mater.,* vol. 5, p. 1500589, 2015.

[37] M. R. Lukatskaya, S. Kota, Z. Lin, M.-Q. Zhao, N. Shpigel, M. D. Levi, J. Halim, J.-L. Taberna, M. W. Barsoum, P. Simon and Y. Gogotsi, "Ultra-high-rate pseudocapacitive energy storage in two-dimensional transition metal carbides," *Nat. Energy,* vol. 2, p. 17105, 2017.

[38] S. Buller, "Modeling the Dynamic Behavior of Supercapacitors Using Impedance Spectroscopy," *IEEE Trans. Ind. Appl.,* vol. 38, no. 6, pp. 1622-1626, 2002.

[39] G. Navarro, J. Najera, J. Torres, M. Blanco, M. Santos and M. Lafoz, "Development and Experimental Validation of a Supercapacitor Frequency Domain Model for Industrial Energy

Applications Considering Dynamic Behaviour at High Frequencies," *Energies,* vol. 13, p. 1156, 2020.

[40] S. M. Rezaei Niya and M. Hoorfar, "On a possible origin of the constant phase element," *Electrochim. Acta,* vol. 188, pp. 98-102, 2016.

[41] R. S. M. Niya and M. Hoorfar, "On a possible origin of the constant phase element," *Electrochim. Acta,* vol. 188, pp. 98-102, 2016.

[42] R. De Levie, "The influence of surface roughness of solid electrode on electrochemical measurements," *Electrochim. Acta,* vol. 10, no. 2, pp. 113-130, 1965.

[43] M. E. Orazem and B. Tribollet, Electrochemical Impedance Spectroscopy, New Jersey: Wiley, 2014.

[44] L. Nyikos and T. Pajkossy, "Fractal dimension and fractional power frequency-dependent impedance of blocking electrodes," *Elektrochim. Acta,* vol. 30, no. 11, pp. 1533-1540, 1985.

[45] B. Sapoval, "Linear and non-linear behavior of fractal and irregular electrodes," *Solid State Ionics,* vol. 75, pp. 269-273, 1995.

[46] H. K. Song, H. Y. Hwang, K. H. Lee and L. H. Dao, "The effect of pore size distribution on the frequency dispersion of porous electrodes," *Electrochim. Acta,* vol. 45, no. 14, pp. 2241-2257, 2000.